

Servo Integrated Nonlinear Model Predictive Control for Overactuated Tiltable-Quadrotors

Jinjie Li, Junichiro Sugihara, and Moju Zhao, *Member, IEEE*

Abstract—Quadrotors are widely employed across various domains, yet the conventional type faces limitations due to underactuation, where attitude control is closely tied to positional adjustments. In contrast, quadrotors equipped with tiltable rotors offer overactuation, empowering them to track both position and attitude trajectories. However, the nonlinear dynamics of the drone body and the sluggish response of tilting servos pose challenges for conventional cascade controllers. In this study, we propose a control methodology for tilting-rotor quadrotors based on nonlinear model predictive control (NMPC). Unlike conventional approaches, our method preserves the full dynamics without simplification and utilizes actuator commands directly as control inputs. Notably, we incorporate a first-order servo model within the NMPC framework. Through simulation, we observe that integrating the servo dynamics not only enhances control performance but also accelerates convergence. To assess the efficacy of our approach, we fabricate a tiltable-quadrotor and deploy the algorithm onboard at a frequency of 100Hz. Extensive real-world experiments demonstrate rapid, robust, and smooth pose tracking performance.

Index Terms—Aerial Systems; Mechanics and Control, Motion Control, Overactuation, MPC

I. INTRODUCTION

AERIAL robots have increasingly attracted attentions due to their mobility in three-dimensional space. As the most popular aerial robot, quadrotors have been applied in various areas including transportation, inspection, and search & rescue [1]. Traditional quadrotors are *underactuated*, meaning that the number of the independent control input (i.e., the rotation speed of four vertically oriented rotors) is fewer than the required six degree-of-freedom (DoF) for full-pose motion, leading to the close relation between attitude and position. However, numerous applications require independent attitude control, particularly in the field of aerial manipulation [2].

To overcome the challenges associated with *underactuation*, researchers have developed two primary ways to achieve *fullactuation* or *overactuation* in rotor-based aerial robots. One way involves adding rotors with fixed tilting angles [3], [4], named as *fixed-rotor* robots. While these robots maintain mechanical and control simplicity comparable to their underactuated counterparts, they encounter issues like constant internal forces, reduced efficiency, and constrained wrench generation in certain directions. Alternatively, the *tilt-rotor* design introduces servo modules to vary thrust directions, enhancing force distribution and energy efficiency. Moreover,

J. Li, and M. Zhao (Corresponding author) are with the DRAGON Lab at the Department of Mechanical Engineering, the University of Tokyo, Tokyo, 113-8654, Japan {jinjie-li, chou}@dragon.t.u-tokyo.ac.jp

J. Sugihara is with the JSK Lab at the Department of Mechano-Informatics, the University of Tokyo, Tokyo, 113-8654, Japan j-sugihara@jsk.imi.i.u-tokyo.ac.jp

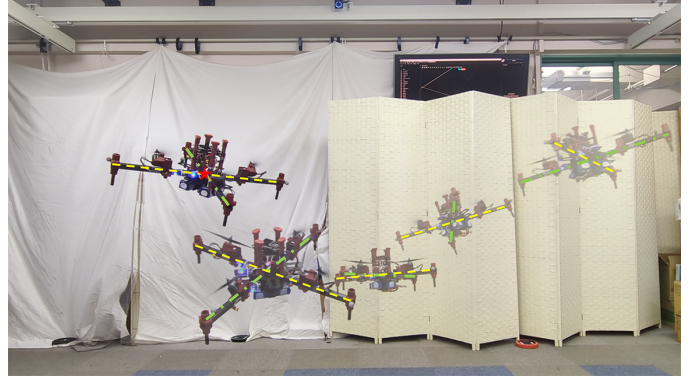


Fig. 1. Our self-made tiltable-quadrotor is tracking a pose trajectory based on the proposed NMPC method. It demonstrates the capability for independent variation in position and attitude to track different Lemniscate curves.

tilt-rotor systems offer the capacity for omnidirectional flight [5], unlocking new potentials in maneuverability and application. Given these advantages, our research focuses on the tiltable-quadrotor, as exemplified in Fig. 1.

The first real-world flight of a quadrotor equipped with tiltable rotors was achieved by Ryll et al., where the control approach is detailed in [6]. Subsequently, the Voliro project [7] introduced a hexacopter with tiltable rotors, marking a pioneering step towards real-world omnidirectional flight. In addition, Senkul et al. [8] developed a quadrotor capable of tilting its rotors along two axes, but they assumed the same thrust generation across all rotors, restricting the vehicle's maneuverability. Despite these advantages, the flight control for tiltable-multirotor remains challenging.

The control complexity of tiltable-multirotors arises primarily from two factors. First, the introduction of additional DoFs to vary tilting angles significantly increases the system's nonlinearity. These extra DoFs make the system overactuated, resulting in multiple solutions in control allocation. Second, the inherent dynamics of tilting servos impede prompt motion change for reference tracking. This slow property can be caused by backlash-induced dead time and the servo's large time constant, which have been reported as critical factor to flight stability [6]. Similar challenges have been observed in other servo-equipped aerial robots, such as SPIDAR [9] and Perching Arm [10].

To address the first challenge, plenty of research have simplified this complex control problem by decoupling into control and allocation components as depicted in Fig. 2a. For control, various strategies based on established control theories have been proposed, including feedback linearization [6], nonlinear inverse dynamics [11], cascade PID [7], LQRI [12], and NMPC [13]. For allocation, Moore–Penrose inverse is typically utilized to map control inputs to specific actuator

commands. While these approaches demonstrate efficacy in real-world flights, their cascaded structure may not fully leverage the potential of overactuated systems or elegantly address actuator constraints. To overcome these drawbacks, recent studies begin to integrate control and allocation within a single optimization framework, notably through nonlinear model predictive control (NMPC). This integrated approach has shown promise in conventional quadrotors [14], [15] and is gaining traction for tiltable-multirotors. For instance, Bicego et al. [16] proposed an NMPC framework suitable for various multi-rotor designs, tested on a hexrotor that all motor tilting for the same angle. However, its applicability to drones with independently tiltable rotors remains unverified. Shawky et al. [17] developed an NMPC controller for tiltable hexarotors, albeit only validated in Gazebo simulation. Despite these advancements, the deployment of unified NMPC in real-world tiltable-multirotors is scarcely reported, and thus one highlight in this work is the implementation on a real tiltable-quadrotor.

To address the second challenge, some studies [7], [17] have chosen to overlook the servo effect, which consequently reduce control performance. Ryll et al. [6] bypassed the issue of dead time by using desired instead of measured angles, and implemented a Smith predictor to address the slow servo response. Although effective, this method is complicated as conventional feedback controllers lack predictive property. In contrast, NMPC inherently incorporates prediction, offering an advantageous framework for addressing delayed servo responses. One approach to indirectly consider servomechanism within NMPC is to confine the change rate of resultant wrench, a method proposed by Brunner et al. [13]. While this technique helps manage the servo dynamics, it cannot accurately capture the entire scope of servo behavior. More recent studies [16], [18] integrated the servo model more explicitly by using the derivative of servo angle as a control input. However, this approach, while it moderates the rate of angle change, is unable to comprehensively account for the nuances of dead time and first-order model. Therefore, our work directly consider the servo dynamics inside the NMPC pipeline.

In this work, we introduce a unified nonlinear model predictive control approach for tiltable-quadrotors, as illustrated in 2b. This approach leverages allocation as an external reference, rather than as an module within the control loop. Our method fully incorporates the nonlinear dynamics into the NMPC framework, directly selecting thrust and servo angle as control inputs. Furthermore, we explicitly integrate the servo dynamics within the model. We find that the inclusion of servo dynamics not only improves model fidelity but also facilitates more rapid convergence of the optimizer.

The main contributions of this article are:

- 1) We propose an NMPC framework for tiltable-quadrotors, which considers the full dynamics and actuator constraints.
- 2) We explicitly consider the servo dynamics inside the NMPC model, which is verified critical for both performance and convergence.
- 3) The control method is implemented onboard with 100Hz control frequency. As far as the author's best knowledge,

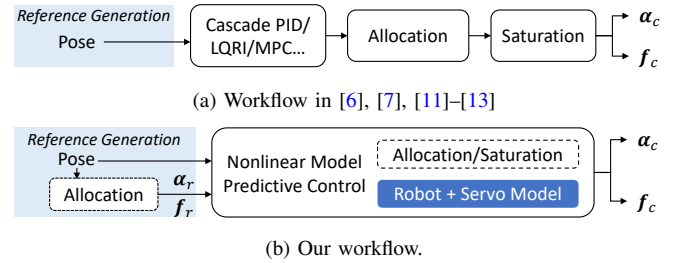


Fig. 2. Comparative analysis of the previous and proposed workflows. Unlike the previous cascade structure, the proposed method directly integrates allocation and constraints within the NMPC optimization process. Furthermore, we explicitly model the servo dynamics. This approach has no simplification on the robot model, resulting in the full exploration of the hardware potential.

this is the first time an actuator-level NMPC is implemented on real tiltable-quadrotors.

The remainder of the article is organized as follows. The modelling for the tiltable-quadrotor is introduced in Section II. The control approach is presented in Section III, followed by simulation analysis in Section IV. We then show the experimental results in Section V and finally the conclusion in Section VI.

II. MODELLING

A. Coordinate Systems and Notation

We denote scalars in unbold x , $X \in \mathbb{R}$, vectors in bold lowercase $\mathbf{x} \in \mathbb{R}^n$, and matrices in bold uppercase $\mathbf{X} \in \mathbb{R}^{n \times m}$. We use $\hat{\cdot}$ to denote estimated values. A vector in $\{\mathcal{W}\}$ can be denoted as ${}^W \mathbf{p}$, and the rotation from $\{\mathcal{G}\}$ to $\{\mathcal{W}\}$ is denoted as ${}^W_G \mathbf{R}$ (rotation matrix) or ${}^W_G \mathbf{q} = [q_w, q_x, q_y, q_z]^T$ (attitude quaternion).

Depicted in Fig. 3, the coordinate systems contain the world inertial frame $\{\mathcal{W}\}$, the body frame $\{\mathcal{G}\}$ whose origin is at the center of gravity (CoG), as well as the i th arm-end frame $\{\mathcal{E}_i\}$ and rotor frame $\{\mathcal{R}_i\}$ ($i = 1, 2, 3, 4$). The origin of $\{\mathcal{E}_i\}$ is positioned at the extremity of the i th arm, where its X axis points outward, and its Z axis aligns parallel to the Z axis of $\{\mathcal{G}\}$. Frame $\{\mathcal{R}_i\}$ is derived from $\{\mathcal{E}_i\}$ through a rotation about the X axis, with the rotation angle denoted as α_i .

B. Tiltable-Quadrotor Model

The model for a tiltable-quadrotor consists of three parts. First, we establish the force and torque model generated by rotors. Then we apply this wrench to the rigid-body dynamics

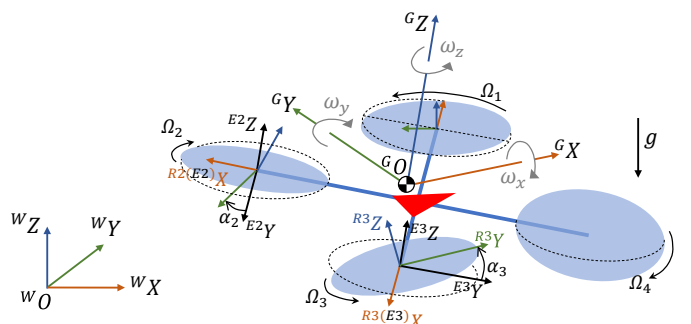


Fig. 3. Diagram of a tiltable-quadrotor with the ENU (X East, Y North, Z Up) inertial frame and the FLU (X Forward, Y Left, Z Up) body frame.

to obtain the full robot model. Finally, we introduce a first-order model to explicitly describe the servo dynamics.

1) *Rotor Wrench Model*: In order to make the established model more general, we assume that N_p rotors are fixed on the robot, and we use d_i (whose value is ± 1) to denote the rotating direction of i th motor and ${}^G\mathbf{p}_{r_i}$ to denote the rotor's position in $\{\mathcal{G}\}$.

Motors rotate their propellers to generate thrust and torque. Here we neglect the angular acceleration of rotors and adopt commonly-used quadratic fit to describe the motor dynamics

$$f_i = k_t \Omega_i^2, \quad \tau_i = k_q \Omega_i^2, \quad (1)$$

where Ω_i is the rotating speed of the i th propeller, k_t and k_q are coefficients identified from experiments. It is assumed that the motors are able to achieve this rotation speed Ω_i with negligible transients.

If we use $\mathbf{f}_c = [f_1, \dots, f_{N_p}]^T$ as input and try to express the thrust and torque in the rotor frame, the wrench becomes

$${}^{R_i}\mathbf{f}_i = [0, 0, f_i]^T, \quad f_i \in [f_{i,\min}, f_{i,\max}], \quad (2)$$

$${}^{R_i}\boldsymbol{\tau}_i = \left[0, 0, -d_i f_i \frac{k_q}{k_t} \right]^T, \quad (3)$$

Based on the coordinate systems, α_i influences the rotation from $\{\mathcal{R}_i\}$ to $\{\mathcal{E}_i\}$ along X axis with denotation as

$${}^{E_i}\mathbf{R} = \mathbf{R}_X(\alpha_i), \quad \alpha_i \in [\alpha_{i,\min}, \alpha_{i,\max}]. \quad (4)$$

In addition to the established torque, tilting a rotating propeller can generate an additional torque caused by gyroscopic effects. For aerial robot with small size, this effect is 2-3 orders of magnitude smaller [16] and can be treated as high-order terms to neglect. Then the resultant force and torque generated by propellers are derived as

$${}^G\mathbf{f}_u = \sum_{i=1}^{N_p} {}^G\mathbf{R}_{E_i} {}^{E_i}\mathbf{R}_{R_i} {}^{R_i}\mathbf{f}_i, \quad (5)$$

$${}^G\boldsymbol{\tau}_u = \sum_{i=1}^{N_p} \left({}^G\mathbf{R}_{E_i} {}^{E_i}\mathbf{R}_{R_i} {}^{R_i}\boldsymbol{\tau}_i + {}^G\mathbf{p}_{r_i} \times {}^G\mathbf{R}_{E_i} {}^{E_i}\mathbf{R}_{R_i} {}^{R_i}\mathbf{f}_i \right), \quad (6)$$

where ${}^G\mathbf{R}_{E_i}$ can be obtained from geometric properties.

2) *Servo Model*: The servo can be modeled with angle, angular velocity or even torque as input. Considering most low-cost servos only support angle control, we hereby model the servo's motion as a first-order damping model

$$\dot{\boldsymbol{\alpha}} = \frac{1}{t_{\text{servo}}} (\boldsymbol{\alpha}_c - \boldsymbol{\alpha}), \quad (7)$$

where $\boldsymbol{\alpha} = [\alpha_1, \alpha_2, \dots, \alpha_{N_p}]^T$ denotes the vector including all servo angles, and $\boldsymbol{\alpha}_c = [\alpha_{c1}, \alpha_{c2}, \dots, \alpha_{cN_p}]^T$ is the symbol for control command.

3) *Rigid-Body Model*: Neglecting the aerodynamic drag during flying, the motion of robot is caused only by gravitational force and rotor wrench. Using position ${}^W\mathbf{p}$, velocity ${}^W\mathbf{v}$, quaternion ${}^W\mathbf{q}$, and angular velocity ${}^G\boldsymbol{\omega}$ (angular velocity of $\{\mathcal{G}\}$ w.r.t $\{\mathcal{W}\}$ and expressed in $\{\mathcal{G}\}$) as states, a six DoF rigid body dynamics can be established as follows

$${}^W\dot{\mathbf{p}} = {}^W\mathbf{v}, \quad (8)$$

$${}^W\dot{\mathbf{v}} = ({}^W\mathbf{R}(\mathbf{q}) {}^G\mathbf{f}_u + {}^W\mathbf{f}_d) / m + {}^W\mathbf{g}, \quad (9)$$

$${}^G\dot{\mathbf{q}} = \frac{1}{2} {}^G\mathbf{q} \circ \mathcal{H}({}^G\boldsymbol{\omega}), \quad (10)$$

$${}^G\dot{\boldsymbol{\omega}} = \mathbf{I}^{-1} (-{}^G\boldsymbol{\omega} \times (\mathbf{I} {}^G\boldsymbol{\omega}) + {}^G\boldsymbol{\tau}_u + {}^G\boldsymbol{\tau}_d), \quad (11)$$

where $\mathbf{R}(\mathbf{q})$ denotes the rotation matrix converted from quaternion, \circ refers to quaternion multiplication, $\mathcal{H}(\cdot)$ means homogenizing a 3D vector $\mathcal{H}(\mathbf{p}) := [0, \mathbf{p}]^T$, ${}^G\mathbf{f}_u$ and ${}^G\boldsymbol{\tau}_u$ are expressed in eqs. (5) and (6), ${}^W\mathbf{f}_d$ and ${}^G\boldsymbol{\tau}_d$ are the force and torque caused by disturbances, as well as m , ${}^W\mathbf{g} = [0, 0, -g]^T$, and \mathbf{I} are the mass, the gravity vector, and the inertia matrix, respectively.

The whole model established above are utilized for control and simulation. Note that this model is created for multirotors, and the tiltable-quadrotor is the special case when $N_p = 4$.

III. CONTROL

Unlike some cascade control algorithms, our proposed NMPC controller leverages the full nonlinear dynamics as the control model, emphasizing a concise and elegant "end-to-end" style. During this section, we first describe the generation of control reference in Section III-A. Then this target is converted into a cost function inside a finite-time optimal control problem (OCP), which is the core concept of NMPC in Section III-B. One drawback of NMPC is its sensitivity to model error, which leads to steady-state error during flight. To solve this problem, a simple integral mechanism is introduced in Section III-C.

A. Generation of Control Reference

Although the NMPC controller is able to work with only ${}^W\mathbf{p}_r$ and ${}^W\mathbf{q}_r$, the optimizer can converge faster by computing reference states as comprehensively as possible. Considering that the computation cost is trivial, this calculation is worthwhile. Thus, all our subsequent experiments are conducted with the full-state reference, and the generation method is introduced here.

Compared with normal quadrotors, tiltable-quadrotors are able to independently track three-dimensional attitude at the same time. Hence, we need both reference position ${}^W\mathbf{p}_r$ and attitude ${}^W\mathbf{q}_r$ as control target. Another difference in control reference comes from the number, where NMPC requires a sequence of reference points as the control target, not just one point for traditional feedback controllers.

The control task can be divided into two types: tracking a constant point or tracking a trajectory. In our system, if the robot tracks a constant point, then all reference points are set as the same, and the reference velocity ${}^W\mathbf{v}_r$, acceleration ${}^W\dot{\mathbf{v}}_r$,

angular velocity ${}^G\boldsymbol{\omega}_r$, and angular acceleration ${}^G\dot{\boldsymbol{\omega}}_r$ are set to zero. Although the research [19] claims that adding the point to the end of the reference can make optimizer easier to find a solution, we find it slows response speed. For tracking a trajectory, the reference points are calculated with a shifting prediction time interval, and ${}^W\mathbf{v}_r$, ${}^G\boldsymbol{\omega}_r$, ${}^W\dot{\mathbf{v}}_r$, and ${}^G\dot{\boldsymbol{\omega}}_r$ can be calculated by differentiating position and attitude. Then the desired ${}^G\mathbf{f}_{u,r}$ and ${}^G\boldsymbol{\tau}_{u,r}$ can be calculated from eqs. (9) and (11).

On the basis of these states, we can obtain the reference thrust $f_{i,r}$ and servo angle $\alpha_{i,r}$ through control allocation. The relations between reference wrench and a group of virtual input \mathbf{z} can be expressed as

$$[{}^G\mathbf{f}_{u,r}, {}^G\boldsymbol{\tau}_{u,r}]^T = \mathbf{A} \mathbf{z}, \quad \text{where} \quad (12)$$

$$\mathbf{z} = \begin{bmatrix} f_{1,r,h} \\ f_{1,r,v} \\ \vdots \\ f_{N_p,r,h} \\ f_{N_p,r,v} \end{bmatrix} = \begin{bmatrix} f_{1,r} \sin \alpha_{1,r} \\ f_{1,r} \cos \alpha_{1,r} \\ \vdots \\ f_{N_p,r} \sin \alpha_{N_p,r} \\ f_{N_p,r} \cos \alpha_{N_p,r} \end{bmatrix}, \quad (13)$$

where the allocation matrix \mathbf{A} can be derived from eqs. (5) and (6) using symbolic computation tools. Then we can calculate $f_{i,r}$ and $\alpha_{i,r}$ as follows

$$\mathbf{z} = \mathbf{A}^\dagger [{}^G\mathbf{f}_{u,r}, {}^G\boldsymbol{\tau}_{u,r}]^T, \quad (14)$$

$$f_{i,r} = \sqrt{f_{i,r,h}^2 + f_{i,r,v}^2}, \quad (15)$$

$$\alpha_{i,r} = \text{atan2}(f_{i,r,h}, f_{i,r,v}), \quad (16)$$

where $(\cdot)^\dagger$ means the Moore–Penrose inverse operation. Note that \mathbf{A}^\dagger is unchanged and only needs to compute once.

B. Nonlinear Model Predictive Control

Nonlinear model predictive control converts the control problem to a constrained nonlinear optimization problem. For quadrotors, depending on the coordinate space, we can choose either a nonlinear model with linear constraints and a simple cost function, or a linear model with nonlinear constraints and a complex cost function. The former is easier to understand while the latter may have advantages in computation speed (please read [20] for some discussions about normal quadrotors). Considering that the former one is more intuitive and has been deployed onboard successfully in many latest research [14], [15], we select the nonlinear model version.

We select the state as $\mathbf{x} = [{}^W\mathbf{p}, {}^W\mathbf{v}, {}^W_G\mathbf{q}, {}^G\boldsymbol{\omega}, \boldsymbol{\alpha}]^T$ and the control input as $\mathbf{u} = [\mathbf{f}_c, \boldsymbol{\alpha}_c]^T$. Given the reference \mathbf{x}_r , \mathbf{u}_r , we define the state error as $\bar{\mathbf{x}} = [\bar{\mathbf{p}}, \bar{\mathbf{v}}, \mathcal{V}(\mathbf{q}_e), \bar{\boldsymbol{\omega}}, \bar{\boldsymbol{\alpha}}]^T$ and the control input error as $\bar{\mathbf{u}} = [\bar{\mathbf{f}}_c, \bar{\boldsymbol{\alpha}}_c - \boldsymbol{\alpha}]^T$, where the over-line symbol denotes $\bar{(\cdot)} = (\cdot) - (\cdot)_r$ if no special explanation, $\mathcal{V}(\cdot)$ represents the vector part of a quaternion $\mathcal{V}(\mathbf{q}) := [q_x, q_y, q_z]^T$, and $\mathbf{q}_e = \mathbf{q} \circ \mathbf{q}_r^{-1}$ represents the quaternion error. Note that the error term for servo angle command is defined as $\bar{\boldsymbol{\alpha}}_c = \boldsymbol{\alpha}_c - \boldsymbol{\alpha}$ instead of the error w.r.t. reference $\bar{\boldsymbol{\alpha}}'_c = \boldsymbol{\alpha}_c - \boldsymbol{\alpha}_r$, aiming to penalize the right-hand of eq. (7) and avoid the sudden change of servo angle. More analysis is presented in Section IV.

Then the optimal control problem in NMPC can be formulated as follows

$$\text{minimize}_{\mathbf{x}_k, \mathbf{u}_k} \sum_{k=0}^{N-1} (\bar{\mathbf{x}}_k^T \mathbf{Q} \bar{\mathbf{x}}_k + \bar{\mathbf{u}}_k^T \mathbf{R} \bar{\mathbf{u}}_k) + \bar{\mathbf{x}}_N^T \mathbf{Q}_N \bar{\mathbf{x}}_N, \quad (17)$$

$$\text{subject to } \mathbf{x}_{k+1} = f(\mathbf{x}_k, \mathbf{u}_k), \quad k = 0 : N-1, \quad (18)$$

$$\mathbf{x}_0 = \hat{\mathbf{x}}, \quad (19)$$

$$\|v_{x,y,z}\| \leq v_{\text{limit}}, \quad \|\omega_{x,y,z}\| \leq \omega_{\text{limit}}, \quad (20)$$

$$\mathbf{u}_{\min} \leq \mathbf{u}_k \leq \mathbf{u}_{\max}, \quad (21)$$

where \mathbf{Q} , \mathbf{R} , \mathbf{Q}_N are positive diagonal matrices representing weights for state cost, control energy cost, and terminal cost, respectively. The eq. (18) indicates the dynamics constraint, where $f(\cdot)$ refers to the full tiltable-quadrotor model established from eq. (2-11). This model is discretized by the *fourth-order Runge–Kutta* method with t_{integ} integrating time. The eq. (19) denotes the initial value constraint, a critical component for feedback in NMPC, wherein $\hat{\mathbf{x}}$ represents the estimated state obtained from the estimator. Finally, the eqs. (20) and (21) refer to the state and input constraints, respectively, which is mainly decided from physical limits and safety concern.

Equation 17 is an nonlinear least-square cost function, where the nonlinearity comes from quaternions. Recall the quaternion error is denoted as $\mathbf{q}_e = \mathbf{q} \circ \mathbf{q}_r^{-1}$, then its cost term can be written as

$$\bar{\mathbf{q}}_k^T \mathbf{Q}_q \bar{\mathbf{q}}_k = \|\text{sgn}(q_{e,w}) \cdot \mathcal{V}(\mathbf{q}_e)\|_{\mathbf{Q}}^2 = \mathcal{V}(\mathbf{q}_e)^T \mathbf{Q}_q \mathcal{V}(\mathbf{q}_e). \quad (22)$$

When NMPC is executing, the finite-time OCP problem defined above is solved during each control loop in t_s frequency, and traditionally the first control command is extracted from the optimal sequence as the control input. However, this way neglects the time caused by NMPC computation and other delay factors, making the command out-of-date. To address this challenge, recognizing the nonlinearity is small within short time intervals, we predict the control command forward using linear interpolation as follows

$$\mathbf{u}_{\text{now}} = \frac{t_s + t_d}{t_{\text{integ}}} (\mathbf{u}_1^* - \mathbf{u}_0^*) + \mathbf{u}_0^*, \quad (23)$$

where \mathbf{u}_0^* and \mathbf{u}_1^* are the first two commands from the generated control sequence, t_s is the time for control loop, t_d is the dead time of actuators, and t_{integ} is the time for one prediction step. At the beginning of the next control loop, the final input \mathbf{u}_{now} is transmitted to low-level autopilot for execution.

In implementation, we leverage several common techniques in NMPC community to accelerate computation. Specifically, *warm-starting*, *real-time iteration (RTI)*, and *multiple-shooting* are adopted. The *warm-starting* tries to accelerate by giving an initial guess near the final solution, where the guess comes from the last round's solution. The RTI only calculates the sequential quadratic programming (SQP) once in one control iteration, preferring speed instead of optimality. Finally, the *multiple-shooting* divides the original OCP into several smaller optimization problems and try to solve them in parallel. We recommend [19] to interested readers for more details.

C. Integral Term for Model Error

To alleviate the influence of model error to NMPC, we adopt an integral term as follows to compensate for pose error

$${}^W \mathbf{f}_d = \text{ITerm}({}^W \hat{\mathbf{p}} - {}^W \mathbf{p}_r), \quad (24)$$

$${}^G \boldsymbol{\tau}_d = \text{ITerm}(\text{sgn}(q_{e,w}) \cdot \mathcal{V}(\hat{\mathbf{q}} \circ \mathbf{q}_r^{-1})), \quad (25)$$

where $\text{sgn}(\cdot)$ denotes sign function. The digital implementation of integral term $u[k+1] = \text{ITerm}(e[k+1])$ with trapezoidal rule and anti-windup is given as [21]

$$\begin{aligned} I'[k+1] &= I[k] + \frac{t_s}{2} (e[k] + e[k+1]), \\ u'[k+1] &= k_I I'[k+1], \\ u[k+1] &= \max(\min(u'[k+1], u_{\max}), u_{\min}), \\ I[k+1] &= I'[k+1] + \frac{1}{k_I} (u[k+1] - u'[k+1]). \end{aligned} \quad (26)$$

The compensating wrench ${}^W \mathbf{f}_d$, ${}^G \boldsymbol{\tau}_d$ is calculated before each NMPC running and then transmitted as inputs into the optimization process through eqs. (9) and (11).

IV. SIMULATION

In this section, we present simulation results to reveal the impact of different NMPC designs on the final performance. To eliminate the influence of model error, disturbance, and other unknown effects, we implement an ideal simulation environment without model error and noise. In the subsequent comparisons, we choose the control frequency as 100Hz to align with real-world experiments, and we choose the simulation frequency as 200Hz since our estimator for real robot is running at this frequency. The simulating model is always the full nonlinear model with servo dynamics eq. (2-11). The weights are all set as Table I if no special explanation.

A. The Effect of Servo Dynamics to Convergence

Aiming to explore the effect of servo dynamics eq. (7) to NMPC, we implement two kinds of NMPC: one has no servo dynamics and hence has no servo angle in states, as well as the other one includes servo dynamics. Two NMPC controllers are commanded to takeoff and reach 1m in height. The result is shown in Fig. 4.

It is natural to think that adding a model increases the OCP complexity, resulting higher difficulty in convergence. However, as revealed by Fig. 4, the NMPC with servo model achieves less oscillation and faster convergence. We believe this is due to the narrower search space implicitly introduced by the first-order servo model. Without this model, the next servo angle command can be any value within the physical limits. With this model, the command is limited in the nearby area of the real servo angle, and this extra limitation accelerates the convergence. For the accuracy of time constant, too short value reduces the narrowing effect and leads to oscillation in Fig. 4d, while the correct or larger values achieves the similar response shown in Fig. 4c. Although the no-servo version achieves convergence in the end, we report that it diverges and crashes in noise-existed Gazebo simulation, not mention in real world. Hence, the inclusion of servo model is not only a plus for control performance, but also a must to achieve real-world usage.

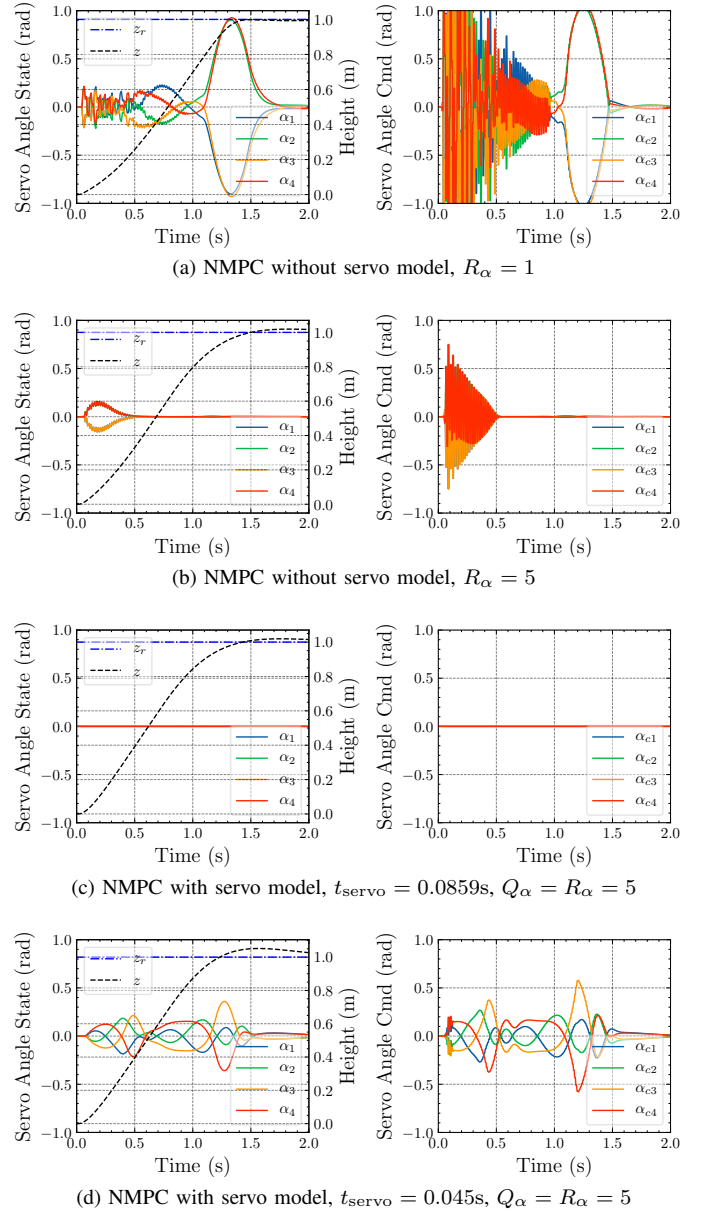


Fig. 4. Comparative analysis of NMPC performance with and without the servo model during a takeoff mission. The actual t_{servo} in simulation is always 0.0859s. Figure (a) and (b) demonstrate that increasing the cost for servo commands mitigates oscillation. Figure (b) and (c) illustrate that incorporating the servo model results in smoother controller performance. However, as shown in (d), an overly small t_{servo} can hinder the NMPC's convergence.

B. The Effect of Servo Dynamics Cost

We want to compare the result of traditional cost $\bar{\alpha}'_c = \alpha_c - \alpha_r$ and our proposed cost $\bar{\alpha}_c = \alpha_c - \alpha$ under the influence of inaccurate α_r . This inaccuracy happens in reality due to the model error or the absent of allocation module. We set the reference $\alpha_r = \mathbf{0}$, set $Q_\alpha = 1$, and try to use NMPC to track the attitude change. The result is presented in Fig. 5.

From the figure, the tracking error of old cost is sensitive to R_α , while the new cost always maintains a small error. The traditional setting ($\bar{\alpha}'_c = \alpha_c - \alpha_r$ and $\bar{\alpha} = \alpha - \alpha_r$) mixes two missions in $\bar{\alpha}'_c$: tracking α_r and indirectly reducing the difference with actual angle α . On the contrary, the new setting ($\bar{\alpha}_c = \alpha_c - \alpha$ and $\bar{\alpha} = \alpha - \alpha_r$) makes $\bar{\alpha}_c$ only

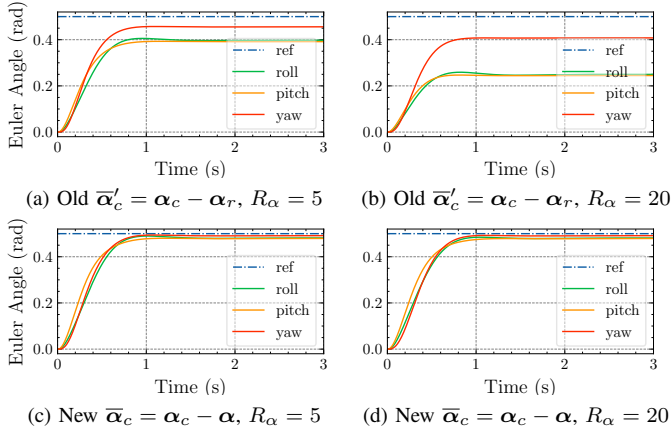


Fig. 5. Comparison of orientation tracking performance with inaccurate α_r . Compared with the old cost function, the new cost effectively mitigates the adverse effect of inaccuracies in α_r .

control the difference with α , and purely leaves the tracking task to $\bar{\alpha}$. If the reference α is accurate, two settings achieve the same performance. Yet if α is inaccurate, this functional decomposition ensures that a large R_α does not cause large steady error. This is quite supportive when R_α is set to a large number to reduce servo oscillation in real world.

V. EXPERIMENTS

A. Robot Platform

We made a tiltable-quadrotor as shown in Fig. 6 to verify the proposed approach. The robot has 400mm wheelbase and 2.77kg weight, of which the size is suitable for indoor flight. The main modules and their communications are illustrated in Fig. 7. The whole system uses Robot Operating System (ROS) for communication. The main algorithms are running in a Khadas VIM4 onboard computer, which has a 2.2GHz Quad core ARM Cortex-A73 and a 2.0GHz Quad core Cortex-A53 CPU. Then it sends control command to the self-designed flight control unit “Spinal”, which employs a STM32H7 series processor and has been employed in many previous works [9], [10]. Next, “Spinal” sends signals to control actuators. Specifically, we choose a T-Motor F55A PROII 6S 4IN1 ESC with DShot protocol to power four T-Motor AT2814 KV900 motors. Each motor is equipped with a 3-blade 9045 propeller. We select Kondo KRS-3302 as servos.

For state estimation, an IMU is installed on “Spinal”, and its data are filtered in an attitude estimator to obtain roll,

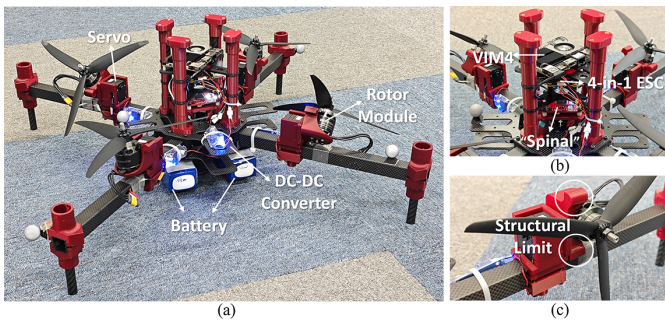


Fig. 6. (a) Snapshot of our self-build tiltable-quadrotor. (b) An onboard computer VIM4, a 4-in-1 electronic speed controller (ESC), and a self-designed flight control unit “Spinal” are centrally mounted on the robot’s body. (c) The feasible servo angle is structurally limited to within $\pm\pi/2$.

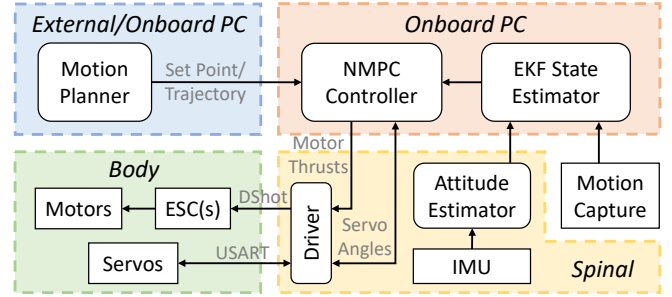


Fig. 7. Diagram of information flow among main modules within our system, where normal rectangles denote hardware modules and rounded rectangles indicate software modules.

pitch angles and attitude velocity. In addition, we use an OptiTrack Motion Capture system to get position and attitude. These measurements are input to an EKF-based state estimator to calculate ${}^W\hat{p}$, ${}^W\hat{v}$, ${}^G\hat{q}$, and ${}^G\hat{\omega}$. The servo angle $\hat{\alpha}$ is directly measured by the Kondo servo without filtering. These estimated states are sent to NMPC for control.

B. Parameter Identification

Model predictive control is sensitive to model parameters, hence we conducted several parameter identification experiments. The identified parameters can be separated into four categories: geometry parameters, inertial parameters, rotor parameters, and servo parameters.

The geometric parameters for the i th rotor ${}^G\mathbf{p}_{ri}$ were directly obtained from the CAD model. The mass parameter was weighted using a weighing scale, and the inertial matrix was identified by the bifilar-pendulum method [22]. The rotor parameters k_t , k_q , $f_{i,\min}$, $f_{i,\max}$ as well as the mapping between command and thrust were identified by an ATI six-axis force/torque sensor installed on a testbed. When identifying rotor parameters, we disassembled one motor from the robot and installed it on the testbed. Comparing this data with the flight performance, we report a 28% lost in thrust due to the aerodynamic interference.

To identify the servo model, we removed propellers for safety, commanded the motor rotating in 60% throttle, and sent a step signal to stimulate the servo to 1.0rad. The data were collected using `rosvbag`, and then the time constant of the servo model was identified by the MATLAB System Identification Toolbox, where we used Prediction Error Minimization as evaluation method. The final result is the average of four servos’ results. Although this no propeller setting may introduce some error compared with the real condition, this

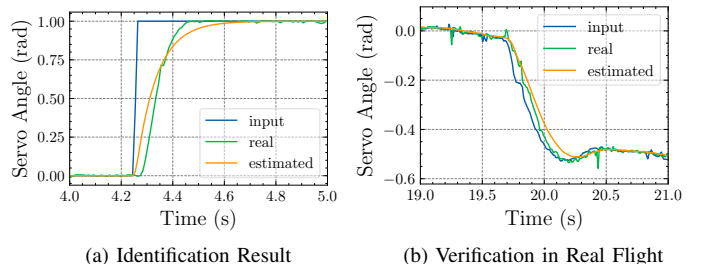


Fig. 8. System identification results for the servo model, achieving an average accuracy of 93.4%.

TABLE I
 MODEL & CONTROL PARAMETERS

Parameter	Value	Parameter	Value	Parameter	Value
N_p	4	k_q/k_t	0.0153	t_{servo}	0.0859s
N	20	t_{integ}	0.1s	t_s	0.01s
$Q_{p,xy}$	300	$Q_{p,z}$	400	$Q_{v,xy}$	10
$Q_{v,z}$	10	$Q_{q,xy}$	300	$Q_{q,z}$	600
$Q_{\omega,xy}$	5	$Q_{\omega,z}$	5	Q_α	5
R_f	1	R_α	250		
v_{limit}	± 1 m/s	ω_{limit}	± 6 rad/s	$\alpha_{i,limit}$	$\pm \pi/2$
$f_{i,min}$	0 N	$f_{i,max}$	30 N	$\alpha_{ci,limit}$	$\pm \pi/2$
$k_{I,xy}$	0	$k_{I,z}$	5	$k_{I,qxy}$	0
$k_{I,qz}$	0	$f_{d,limit}$	5 N	$\tau_{d,limit}$	1 Nm ²

accuracy is enough for the real-world flight as shown in Fig. 8. Rotor and servo parameters are listed in Table I.

C. Tracking Test

The tool *acados* [23] is utilized to solve the NMPC problem, where we use *Partial Condensing HPIPM* as QP solver and *Explicit Runge-Kutta* as integrator. The control parameters are listed in Table I, and the integral term is used only for Z axis.

We conducted three experiments to evaluate the proposed algorithm. Initially, the tiltable-quadrotor took off and then was poked by a stick to test disturbance rejection. Next, we carried out an experiment to track several pose points, aiming to evaluate the performance on physically infeasible trajectory. Finally, the robot was controlled to track a 6-DoF pose trajectory.

1) *Takeoff and Disturbance Rejection*: Takeoff is the basis for all other experiments. During takeoff, the position command $\mathbf{p}_r = [0.0, 0.0, 1.0]^T$ was sent to the robot. After takeoff, the robot entered hovering state and was disturbed by a stick. The experiment snapshots and data are shown in Fig. 9 and Fig. 10, respectively.

As can be seen in Fig. 10, the robot can achieve the target height with 13% overshoot, and then the integral term slowly corrects the Z position to the reference. In addition, the drift of X and Y position is smaller than 0.05m. The error for three-axis attitudes without disturbance are lower than 0.05rad. After giving force to the robot, it can recover to the hovering state, demonstrating the robustness of the proposed controller.

2) *Set-Pose Tracking*: The capability of tracking static points was tested in this experiment, and the reference in each DoF can be seen as a step signal. At the beginning, the pose point $\mathbf{p}_r = [0.3, 0.2, 1.2]^T$, $\mathbf{q}_r = \text{RPY2Quaternion}(0.5, 0.0, 0.3)^T$ was sent to the robot. After eight seconds, another pose point $\mathbf{p}_r = [-0.3, 0.0, 1.0]^T$, $\mathbf{q}_r = \text{RPY2Quaternion}(0.5, 0.5, -0.3)^T$ was sent. After another eight seconds, the robot was commanded to return to the starting point. The result is plotted in Fig. 11.

From Fig. 11, the robot can track the position and attitude change simultaneously due to the non-simplification of the nonlinear robot model. The tracking performances for Z position and Yaw attitude are generally better than other axes. In addition, it can be found that X exceeds the reference for about 0.1m, Y is always 0.2m smaller than reference, and Pitch is 0.3rad lower than target. We infer this is due to aerodynamic inference from tilting rotors and

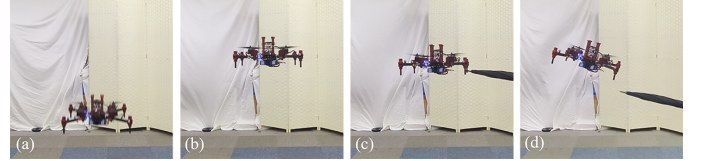


Fig. 9. Sequential snapshots demonstrating the takeoff and disturbance rejection phases of the experiment, showcasing the robustness of the controller.

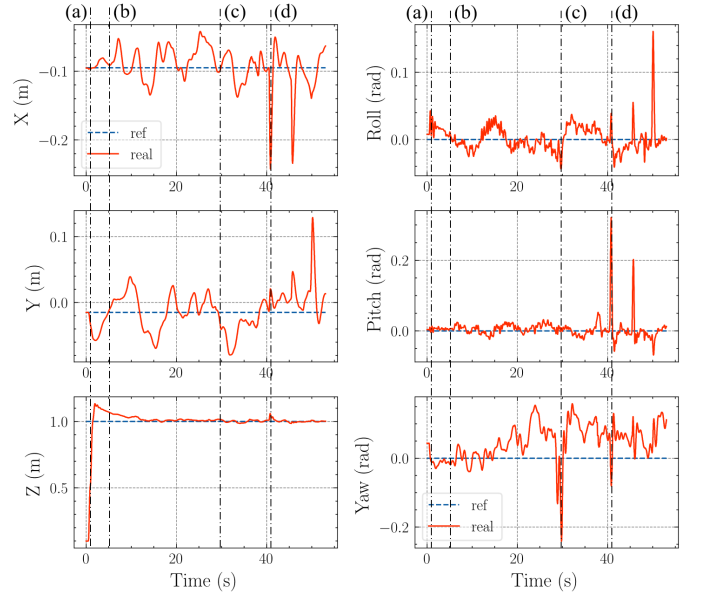


Fig. 10. Pose data from the takeoff and disturbance rejection experiment, where vertical dash-dotted lines indicate corresponding moments in Fig. 9.

model error. Another interesting phenomenon is the oscillation after sending the second point. The second pose point requires longer movement than the first one, making NMPC difficult to find a suitable transition trajectory. This difficulty emphasizes the importance of trajectory planning.

3) *Pose Trajectory Tracking*: Finally, a pose trajectory was sent to the robot. Let $\omega = 2\pi/20$, then the position \mathbf{p}_r

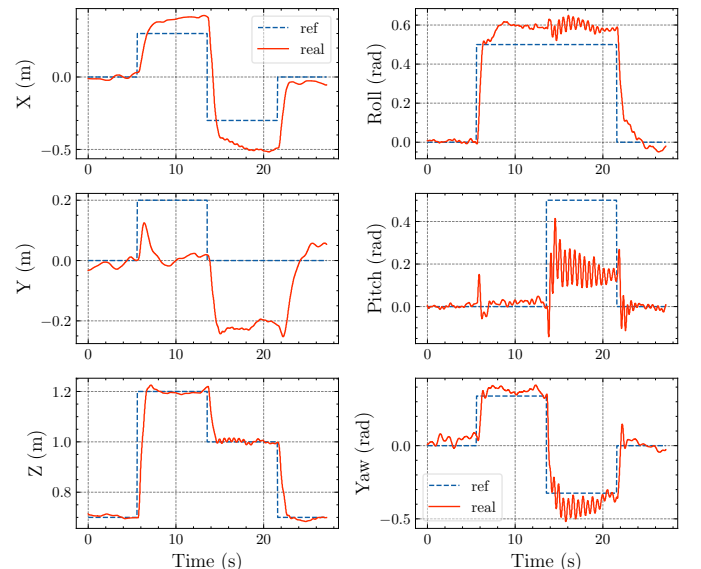


Fig. 11. Pose data from the set point tracking experiment. The robot tracks two pose points and finally goes back to the starting point.

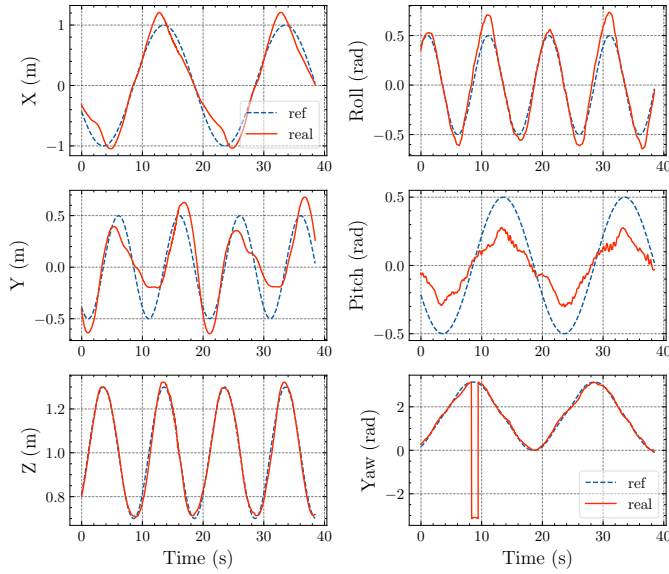


Fig. 12. Pose data from the pose trajectory tracking experiment. The yaw angle is limited in $[-\pi, \pi]$, sometimes resulting in the sudden change. The tracking RMSE for all directions are X: 0.153m, Y: 0.169m, Z: 0.020m; Roll: 0.096rad, Pitch: 0.201rad, Yaw: 0.081rad.

was set as $p_x(t) = \cos(\omega t)$, $p_y(t) = \sin(2\omega t)/2$, $p_z(t) = 0.3 \sin(2\omega t + \pi/2) + 1.0$, as well as the attitude \mathbf{q}_r was set from Euler angle as $roll(t) = -\sin(2\omega t)/2$, $pitch(t) = 0.5 \cos(\omega t)$, $yaw(t) = \pi/2 \cdot \sin(\omega t + \pi) + \pi/2$. The tracking result is displayed in Fig. 12, and the real-world flight snapshot is presented in Fig. 1.

From the figure, the tracking performance for Z and Yaw are better than other directions. It can be noted that the pitch tracking is worse than roll and yaw, which may due to aerodynamic disturbance. To sum up, the proposed method is able to track position and attitude trajectories simultaneously, while the modelling error and aerodynamic effect should be further considered to reduce the tracking error.

VI. CONCLUSION

In this article, we proposed an NMPC-based control framework for tilttable-quadrotors. Leveraging a full nonlinear model with servo dynamics, the method directly generated thrust and servo angle as control input. We found in simulation that the inclusion of servo dynamics not only enhanced the control performance but also assisted in the convergence. Finally, the algorithm was verified in real world using a self-made robot.

During flight, the aerodynamic disturbance caused by tilting rotors remains a severe problem. Although integral term is adopted in this article, this way weakens the response speed, presenting the need for more advanced disturbance rejection method. In addition, the influence of servo dynamics on convergence may require further mathematical explanation.

REFERENCES

- [1] D. Floreano and R. J. Wood, "Science, technology and the future of small autonomous drones," *Nature*, vol. 521, no. 7553, pp. 460–466, May 2015.
- [2] A. Ollero, M. Tognon, A. Suarez, D. Lee, and A. Franchi, "Past, present, and future of aerial robotic manipulators," *IEEE Transactions on Robotics*, vol. 38, no. 1, pp. 626–645, Feb. 2022.

- [3] D. Brescianini and R. D'Andrea, "Design, modeling and control of an omni-directional aerial vehicle," in *Proceedings of IEEE International Conference on Robotics and Automation (ICRA)*, Stockholm, Sweden, May 2016, pp. 3261–3266.
- [4] G. Flores, A. M. De Oca, and A. Flores, "Robust nonlinear control for the fully actuated hexa-rotor: Theory and experiments," *IEEE Control Systems Letters*, vol. 7, pp. 277–282, Jul. 2022.
- [5] M. Hamandi, F. Usai, Q. Sablé, N. Staub, M. Tognon, and A. Franchi, "Design of multirotor aerial vehicles: A taxonomy based on input allocation," *The International Journal of Robotics Research*, vol. 40, no. 8-9, pp. 1015–1044, Aug. 2021.
- [6] M. Ryll, H. H. Bulthoff, and P. R. Giordano, "A novel overactuated quadrotor unmanned aerial vehicle: Modeling, control, and experimental validation," *IEEE Transactions on Control Systems Technology*, vol. 23, no. 2, pp. 540–556, Mar. 2015.
- [7] M. Kamel *et al.*, "The Voliro omniorientational hexacopter: An agile and maneuverable tilttable-rotor aerial vehicle," *IEEE Robotics & Automation Magazine*, vol. 25, no. 4, pp. 34–44, Dec. 2018.
- [8] A. F. Şenkul and E. Altuğ, "System design of a novel tilt-roll rotor quadrotor UAV," *Journal of Intelligent & Robotic Systems*, vol. 84, no. 1-4, pp. 575–599, Dec. 2016.
- [9] M. Zhao, T. Anzai, and T. Nishio, "Design, modeling, and control of a quadruped robot SPIDAR: Spherically vectorable and distributed rotors assisted air-ground quadruped robot," *IEEE Robotics and Automation Letters*, vol. 8, no. 7, pp. 3923–3930, Jul. 2023.
- [10] T. Nishio, M. Zhao, K. Okada, and M. Inaba, "Design, control, and motion planning for a root-perching rotor-distributed manipulator," *IEEE Transactions on Robotics*, vol. 40, pp. 660–676, 2024.
- [11] G. Scholz and G. F. Trommer, "Model based control of a quadrotor with tilttable rotors," *Gyroscope and Navigation*, vol. 7, no. 1, pp. 72–81, Jan. 2016.
- [12] M. Allenspach *et al.*, "Design and optimal control of a tiltrotor micro-aerial vehicle for efficient omnidirectional flight," *The International Journal of Robotics Research*, vol. 39, no. 10-11, pp. 1305–1325, Sep. 2020.
- [13] M. Brunner *et al.*, "Trajectory tracking nonlinear model predictive control for an overactuated MAV," in *Proceedings of IEEE International Conference on Robotics and Automation (ICRA)*, Paris, France, May 2020, pp. 5342–5348.
- [14] S. Sun, A. Romero, P. Foehn, E. Kaufmann, and D. Scaramuzza, "A comparative study of nonlinear MPC and differential-flatness-based control for quadrotor agile flight," *IEEE Transactions on Robotics*, vol. 38, no. 6, pp. 3357–3373, Dec. 2022.
- [15] J. Li, L. Han, H. Yu, Y. Lin, Q. Li, and Z. Ren, "Nonlinear MPC for quadrotors in close-proximity flight with neural network downwash prediction," in *Proceedings of the 62nd IEEE Conference on Decision and Control (CDC)*, Singapore, Singapore, Dec. 2023, pp. 2122–2128.
- [16] D. Bicego, J. Mazzetto, R. Carli, M. Farina, and A. Franchi, "Nonlinear model predictive control with enhanced actuator model for multi-rotor aerial vehicles with generic designs," *Journal of Intelligent & Robotic Systems*, vol. 100, no. 3-4, pp. 1213–1247, Dec. 2020.
- [17] D. Shawky, C. Yao, and K. Janschek, "Nonlinear model predictive control for trajectory tracking of a hexarotor with actively tilttable propellers," in *Proceedings of the 7th International Conference on Automation, Robotics and Applications (ICARA)*, Prague, Czech Republic, Feb. 2021, pp. 128–134.
- [18] M. Brunner, W. Zhang, A. Roumie, M. Tognon, and R. Siegwart, "MPC with learned residual dynamics with application on omnidirectional MAVs," Jul. 2022, arXiv:2207.01451 [cs]. [Online]. Available: <http://arxiv.org/abs/2207.01451>
- [19] S. Gros, M. Zanon, R. Quirynen, A. Bemporad, and M. Diehl, "From linear to nonlinear MPC: bridging the gap via the real-time iteration," *International Journal of Control*, vol. 93, no. 1, pp. 62–80, Jan. 2020.
- [20] M. Greeff and A. P. Schoellig, "Flatness-based model predictive control for quadrotor trajectory tracking," in *Proceedings of IEEE/RSJ International Conference on Intelligent Robots and Systems (IROS)*, Madrid, Spain, 2018, pp. 6740–6745.
- [21] R. W. Beard and T. W. McLain, *Small Unmanned Aircraft: Theory and Practice*. Princeton, NJ, USA: Princeton University Press, Feb. 2012.
- [22] M. R. Jardin and E. R. Mueller, "Optimized measurements of unmanned-air-vehicle mass moment of inertia with a bifilar pendulum," *Journal of Aircraft*, vol. 46, no. 3, pp. 763–775, May 2009.
- [23] R. Verschueren *et al.*, "acados—A modular open-source framework for fast embedded optimal control," *Mathematical Programming Computation*, vol. 14, no. 1, pp. 147–183, Mar. 2022.